Plaquette boson-fermion model of cuprates

Ehud Altman and Assa Auerbach
Department of Physics, Technion, Haifa 32000, Israel
(Received 7 August 2001; published 14 February 2002)

The strongly interacting Hubbard model on the square lattice is reduced to the low energy plaquette boson fermion model (PBFM). The four bosons (an antiferromagnon triplet and a *d*-wave hole pair), and the fermions are defined by the lowest plaquette eigenstates. We apply the contractor renormalization method of Morningstar and Weinstein to compute the boson effective interactions. The range-3 truncation error is found to be very small, signaling short hole-pair and magnon coherence lengths. The pair-hopping and magnon interactions are comparable, which explains the rapid destruction of antiferromagnetic order with emergence of superconductivity, and validates a key assumption of the projected SO(5) theory. A vacuum crossing at larger doping marks a transition into the overdoped regime. With hole fermions occupying small Fermi pockets and Andreev coupled to hole pair bosons, the PBFM yields several testable predictions for photoemission, tunneling asymmetry, and entropy measurements.

DOI: 10.1103/PhysRevB.65.104508 PACS number(s): 74.20.Mn

I. INTRODUCTION

In 1987, shortly after the discovery of high temperature superconductivity in cuprates, Anderson[1] proposed that the key to this perplexing phenomenon hides in the large positive Hubbard interactions in the copper oxide planes. Indeed, at zero hole doping, the Hubbard model captures the Mott insulator physics of the parent compounds, e.g., La_2CuO_4. The doped Hubbard model, however, has so far resisted a definitive solution, primarily because its spins and holes are highly entangled with no obvious small parameter to separate them. Whether the Hubbard model even supports superconductivity without additional interactions remains a subject of controversy. Different mean field theories suggest conflicting ground state order parameters and correlations. Numerical methods are restricted to finite clusters where hole pairing is found,[2–4] but off-diagonal long range order has not been ascertained.

This paper charts a route from the microscopic Hubbard model on the square lattice to an effective lower energy plaquette boson fermion model (PBFM) at low hole doping. We apply the contractor renormalization (CORE) method of Morningstar and Weinstein[5] to the plaquettized lattice (see Fig. 1) in a one step transformation.

We find that the bosonic part of the effective Hamiltonian is closely related to the projected SO(5) [pSO(5)] theory;[6,7] a theory of four bosons: a hole pair and a (antiferro)magnon triplet. The pSO(5) model describes the competition between antiferromagnetism and superconductivity in a quantum mechanical framework. Its mean field theory yields some broad features of the cuprate phase diagram at low doping. At low temperature, the hole pairs are governed by a phase fluctuations action[8,9] which explains the (non BCS) proportionality between superfluid density, transition temperature, and hole concentration. In the superconducting phase, the magnons are massive and give rise to an antiferromagnetic resonance in neutron scattering. These massive magnons were argued to produce a resistance peak series in Josephson junctions.[10]

Nevertheless without a microscopic foundation, the fundamental ''mechanism'' problem remains: What creates and holds together *d*-wave hole pairs in the presence of local repulsive interactions, without the benefit of retardation and phonons? Even assuming that hole pairs move coherently, what is their hopping rate, and is it of the same order as the Heisenberg exchange energy as assumed by the pSO(5) theory?

Here we address these questions and afford the pSO(5) theory and its phase diagram a microscopic foundation. We also include the hole fermions which provide gapless (nodal) excitations in the square lattice. Their band structure is obtained from previously published numerical results, and their coupling to the bosons is estimated by symmetry and microscopic considerations.

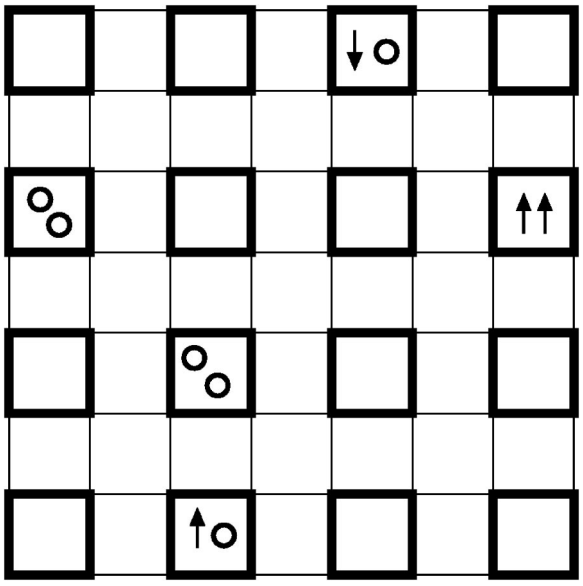

FIG. 1. Local bosons and fermions on the plaquette lattice. The singlet RVB vacua are depicted as solid squares. Holes are depicted by circles. The triplets, single hole and hole pairs Hubbard eigenstates define the degrees of freedom of the effective plaquette boson-fermion model. Interplaquette couplings are computed using contractor renormalization.

The resulting plaquette boson fermion model (PBFM) describes two coupled charged systems (i) Hole pair bosons, which Bose condense below T_c and induce a proximity gap on the holes. (ii) The hole fermions, which occupy small Fermi pockets around $(\pm\pi/2,\pm\pi/2)$ and have a large van Hove peak in density of states near $(\pm\pi,0),(0,\pm\pi)$, the ''antinodal'' points.

We discuss the thermodynamics of the coupled system, with the constraint on the total doping density. Previously proposed boson-fermion models[11] differ from the PBFM by their Hilbert space (e.g., by having a large Fermi surface, and counting occupations from the electron vacuum). For the PBFM, in the weak coupling approximation, some straightforward experimental implications are obtained.

(1) Hole spectral weight in Luttinger theorem-violating momenta (outside the ''large'' electron Fermi surface), e.g., on the line $(\pi,0)\rightarrow(\pi,\pi)$.[12] This weight survives above T_c and is associated with excited holes moving in the correlated RVB vacuum.

(2) Asymmetry in tunneling conductance. At low doping, $x\ll 1$, particle-hole symmetry is expected to be violated, i.e., the positive bias conductance (injection of electrons) is suppressed by a factor proportional to x, relative to the negative bias conductance (injection of holes). Such a trend indeed appears in tunneling data.[13]

(3) The pseudogap doping dependence. The pseudogap energy in photoemission[14,15] and tunneling[13] is at the van Hove peak of antinodal fermions. The decrease of pseudogap with doping follows the increase in fermion chemical potential. Its derivative with respect to doping measures the combined hole fermions' and hole pair bosons' compressibilities.

(4) Nodal transverse velocity. The quasiparticles proximity gap near the nodal directions determines their transverse velocity. This velocity can be measured by photoemission and optical conductivity.[16] We expect it to vanish at T_c, and to be proportional to the Bose condensate order parameter. Thus it should scale as $v_\perp\propto\sqrt{T_c(x)}$.

(5) Hole dependent entropy. At temperatures above the superconducting transition, hole pairs evaporate into hole fermions, because of the difference in their density of states. The doping dependent entropy[17] is dominated by the fermion contribution.

The paper is organized as follows. In Sec. II we introduce the eigenstates of the Hubbard model on a plaquette. The local bosons and fermions are defined as the creation operators of these eigenstates. The physics learned from the four site problem is instructive: Undoped, the ground state is a local resonating valence bonds (or projected d-wave BCS) state. The four bosons create the lowest triplet and the hole pair singlet. There are two degenerate spin half plaquette fermion states with symmetry $(\pi,0)$ and $(0,\pi)$.

It has long been appreciated that in the Hubbard model, two holes cannot bind on a dimer bond, but they can bind on a plaquette (and on larger clusters).[18] The hole pair wave function has $d_{x^2-y^2}$ symmetry for $\pi/2$ rotations. The next step is to compute their interplaquette hopping rate in order to see whether they can preserve their integrity on the infinite square lattice. A short discussion is included about plaquette ''vacuum crossing,'' which occurs at large chemical potentials and may be associated with a transition from underdoped to the overdoped regime.

In Sec. III the contractor renormalization (CORE) method is reviewed. The method requires exact diagonalization of multiplaquette clusters, in principle up to infinite range. Of course, the method is useful only if it converges rapidly in a feasible range of interactions. We have tested the convergence of the low spectrum for the Hubbard models on open ladders, with satisfying results. These tests confirm our belief that the convergence depends on a short boson coherence length, of order one plaquette size. This is very encouraging for the useful application of CORE to our problem, since the experimental superconducting coherence length of cuprates also appears to be particularly short in the underdoped systems. We discuss the artifacts of the *formal* translational symmetry breaking within CORE. In Appendix B, we use the tight binding model as a pedagogical example of how longer range interactions of CORE serve to restore an unphysically broken symmetry.

In Sec. IV the plaquette boson-fermion model is derived. We discuss the hole pairs integrity, as evidenced from the numerical results, and how it is related to the sizeable pair hopping energy. The pair kinetic energy is crucial in stabilizing superconductivity. The full four boson Hamiltonian is given in Appendix A. The hole fermions band structure and interactions with the bosons are added. The thermodynamics of the weakly coupled PBFM yields a relation between the pseudogap energy, the bosons and fermions compressibilities, and the evaporation of hole pairs into fermions at higher temperature. We conclude with a summary and a discussion of future directions in Sec. V.

II. PLAQUETTE STATES

We study the Hubbard model

$$\mathcal{H}=-t\sum_{\langle ij\rangle,s}^{sl}(c_{is}^{\dagger}c_{js}+\text{H.c.})+U\sum_i n_{i\uparrow}n_{i\downarrow}, \tag{1}$$

where $c_{is}^{\dagger}, n_{is}$ are electron creation and number operators at site i on the square lattice. We will occasionally refer to its Gutzwiller projected version, the t-J model

$$\mathcal{H}^{tJ}=-t\mathcal{P}\sum_{\langle ij\rangle,s}(c_{is}^{\dagger}c_{js}+\text{H.c.})\mathcal{P}+J\sum_{\langle ij\rangle}\mathbf{S}_i\cdot\mathbf{S}_j+\mathcal{J}'. \tag{2}$$

$\mathcal{P}$ is the projector of doubly occupied states, and $J\rightarrow 4t^2/U$ at large U/t. $\mathcal{J}'$ is the term of order J that includes next nearest neighbor hole hopping.[19] For one electron per site (half filling), the short range antiferromagnetic correlations are apparent when diagonalizing (1) and (2) on two sites. The dimer states were used to construct effective models on the ladder[20,21] and for spin-Peierls phases on the square lattice.[22] The projected SO(5) model was defined on a ladder using empty dimer states as the hole pair bosons.[6] However, there is *no hole pair binding* for the Hubbard model on a dimer. Naively, this suggests that pairs could readily disintegrate into single holes once interdimer hopping is turned on. Moreover, if one wishes to capture d-wave symmetry in the

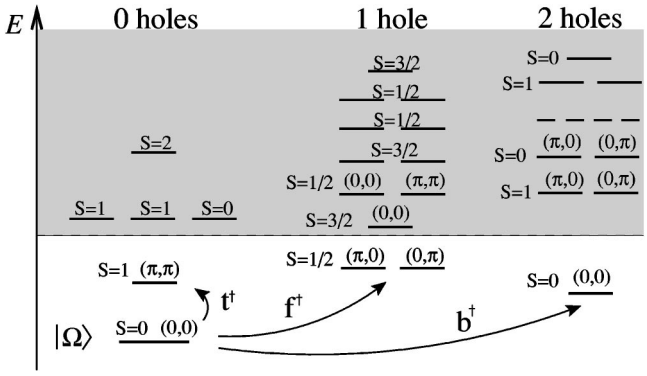

FIG. 2. Lowest spectrum of the Hubbard model on a plaquette. Eigenstates are labeled by total spin S and plaquette momentum $Q_x, Q_y = 0, \pi$. The shaded area is over all high energy truncated states. The vacuum is defined as $|\Omega\rangle$, and the second quantized operators connect the vacuum to the lowest eigenstates as shown.

hole pair wave function, the basic unit block must possess at least fourfold rotational symmetry.

The smallest such block that can cover the square lattice is the four site plaquette. It is a trivial task to diagonalize the Hubbard model on a plaquette and obtain its spectrum and wave functions.

The spectrum is depicted in Fig. 2. Since it is cumbersome to write the full wave functions explicitly, we represent their dominant correlations as follows (i) Real space (RS) description using holes, dimer singlets and dimer triplets as depicted in Fig. 3. (ii) Plaquette momenta (PM) representations using $\mathbf{Q} = (Q_x, Q_y)$, $Q_\alpha = 0, \pi$, the four points on the plaquette Brillouin zone. The electron operator of plaquette i is given by

$$c^\dagger_{\mathbf{Q}is} = \frac{1}{2} \sum_{\eta = 0, \hat{x}, \hat{y}, \hat{x}+\hat{y}} e^{i\mathbf{Q}\cdot\eta} c^\dagger_{i+\eta s}. \tag{3}$$

It is instructive to examine the plaquette eigenstates and energies in some detail before proceeding to couple them.

A. The vacuum

The ground state of the 4-site Hubbard model at half filling ($n_e = 4$) is called $|\Omega\rangle$. In the PM representation it can be described by (suppressing the plaquette index)

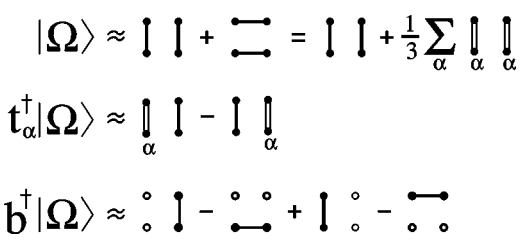

FIG. 3. Real space representation of plaquette bosons. Dominant spin and charge correlations in the plaquette bosons wave functions. Bold lines represent singlet dimers $\uparrow_i\downarrow_j - \downarrow_i\uparrow_j$, and double lines represent the triplet $\uparrow_i\downarrow_j + \downarrow_i\downarrow_j$, $\uparrow_i\uparrow_j \pm \downarrow_i\downarrow_j$, where i and j are on sublattices A and B, respectively. Holes are depicted by open circles.

$$|\Omega\rangle = \frac{\mathcal{P}}{\sqrt{Z_\Omega}} (c^\dagger_{(\pi,0)\uparrow} c^\dagger_{(\pi,0)\downarrow} - c^\dagger_{(0,\pi)\uparrow} c^\dagger_{(0,\pi)\downarrow}) c^\dagger_{(0,0)\uparrow} c^\dagger_{(0,0)\downarrow} |0\rangle. \tag{4}$$

Z is the wave function normalization factor. $|\Omega\rangle$ is a d-wave BCS state, where doubly occupied states are suppressed by a partial Gutzwiller projection $\mathcal{P}(U/t)$. (At large U, $\mathcal{P}$ becomes a full projection.)

In the RS representation, see Fig. 3, $|\Omega\rangle$ is depicted as the resonating valence bonds (RVB) ground state of the Heisenberg model plus small contributions from doubly occupied sites. In the two dimer basis, $|\Omega\rangle$ contains a large contribution from a triplet pair. The product state $|\Omega\rangle = \Pi_i^{\text{plaq}} |\Omega\rangle_i$, is our vacuum state for the full lattice, upon which Fock states can be constructed using second quantized boson and fermion creation operators.

B. Magnon triplet

The magnons are defined by the lowest triplet of $S = 1$ states. In PM representation they are

$$t^\dagger_\alpha |\Omega\rangle = \frac{\mathcal{P}}{\sqrt{Z_t}} \sum_{\mathbf{Q}s} c^\dagger_{\mathbf{Q}s} \sigma^\alpha_{ss'} c_{\mathbf{Q}+(\pi,\pi)s'} |\Omega\rangle, \quad \alpha = x, y, z, \tag{5}$$

where σ^α are Pauli matrices. These (antiferro-)magnons have plaquette momentum $\mathbf{Q} = (\pi, \pi)$. Their excitation energy is close to the superexchange energy $J \approx 4t^2/U$. An antiferromagnetic state can be constructed by a product of plaquette coherent states

$$\Psi^{afm} = \prod_i^{\text{plaq}} (\cos\theta + \sin\theta m^\alpha t^\dagger_{i\alpha}) |\Omega\rangle, \tag{6}$$

where $|\mathbf{m}| = \mathbf{1}$. This state supports a finite staggered moment

$$\frac{1}{N} \langle S^\alpha_{(\pi,\pi)} \rangle_{\theta, m^\alpha} = \sqrt{3/8} m^\alpha \cos\theta \sin\theta \leqslant 0.306. \tag{7}$$

Note that the maximal magnetization per site supported by Ψ^{AFM} is less than the classical value of 0.5, since it does not contain higher spin states up to $S = 2$.

C. Single hole fermions

The ground states for a single hole ($n_e = 3$) are two degenerate doublets described by plaquette momenta $\mathbf{Q} = (0, \pi), (\pi, 0)$:

$$f^\dagger_{\mathbf{Q}s} |\Omega\rangle = \frac{\mathcal{P}}{\sqrt{Z_\mathbf{Q}}} c_{\mathbf{Q}s} + \cdots |\Omega\rangle, \quad s = \uparrow, \downarrow, \tag{8}$$

where $\cdots$ represent higher order electron operators. The hole fermion Bloch state can be constructed as

$$f^\dagger_{\mathbf{k}+\mathbf{Q}s} |\Omega\rangle = \sum_i^{\text{plaq}} e^{i\mathbf{k}\cdot\mathbf{x}_i} f^\dagger_{\mathbf{Q}is} |\Omega\rangle. \tag{9}$$

For a lattice of *disconnected* plaquettes $f^\dagger_{(\pi,0)}$ creates an eigenstate with a photoemission spectral weight given by

$$|\langle\Omega|f_{(\pi,0)s}c_{(\pi,0)s}|\Omega\rangle|^2 = Z_{(\pi,0)}, \tag{10}$$

where, e.g., for the t-J model, $1/4 < Z_{(\pi,0)} < 1/2$ is a function of t/J. This weight is further renormalized by interplaquette couplings in the effective Hamiltonian.

Incidentally, there is another degenerate pair of doublets at higher energy (of order J) at momenta $\mathbf{Q}=(0,0),(\pi,\pi)$. It turns out that by symmetry, the (π,π) state has vanishing hole spectral weight, that is to say for all values of U/t

$$Z_{(\pi,\pi)} = |\langle\Omega|f_{(\pi,\pi)s}c_{(\pi,\pi)s}|\Omega\rangle|^2 = 0. \tag{11}$$

Since these states couple by interplaquette hopping to the lower doublet, this produces an asymmetry of the quasiparticle weight between momenta close to $(0,0)$ and (π,π). This asymmetry may explain the difficulty in observing ''shadow bands,'' i.e., quasiparticles on the Fermi pockets surfaces closer to (π,π).[23]

It is interesting to note that the twofold degeneracy of the fermion doublets is a property of the plaquette. The four site Hubbard and t-J Hamiltonians happen to commute with the plaquette d-density wave operator[24]

$$\hat{D} = i\mathcal{P}\sum_s (c^\dagger_{(\pi,0)s}c_{(0,\pi)s} - c^\dagger_{(0,\pi)s}c_{(\pi,0)s})\mathcal{P}. \tag{12}$$

$\hat{D}$ connects between the doublet pairs $(\pi,0)\leftrightarrow(0,\pi)$ and $(0,0)\leftrightarrow(\pi,\pi)$. Thus a possible ground state of one hole is the current carrying state

$$\Psi_s = \prod_i^{\text{plaq}} (f^\dagger_{(\pi,0),is} + i f^\dagger_{(0,\pi),is})|\Omega\rangle, \tag{13}$$

which is a staggered flux (or d-density wave) state. For a single hole in 4×4 periodic lattices, this state does not seem to be the lowest energy (see Sec. IV D). However, a large susceptibility for such currents is expected since the hole dispersion has a valley between the antinodal points $(\pi,0)$ and $(0,\pi)$, which is weakly dispersive and contains a large admixture of the two plaquette fermion states. It is thus conceivable that the staggered flux combination of the plaquette fermions would be selected in a vortex core or near the sample edge.

D. Hole pair boson

The ground state of two holes $(n_e=2)$ is described by

$$b^\dagger_\alpha|\Omega\rangle = \frac{1}{\sqrt{Z_b}}\mathcal{P}c^\dagger_{(0,0)\uparrow}c^\dagger_{(0,0)\downarrow}|0\rangle$$

$$= \frac{1}{\sqrt{Z'_b}}\left(\sum_{ij} d_{ij}c_{i\uparrow}c_{j\downarrow} + \cdots\right)|\Omega\rangle, \tag{14}$$

where d_{ij} is $+1$ (-1) on vertical (horizontal) bonds, and $\cdots$ are higher order U/t-dependent operators. Thus, $b^\dagger$ creates a pair with internal d-wave symmetry with respect to the vacuum. For the relevant range of U/t, the state normalization is $1/3 < Z'_b < 2/3$. The important energy to note is the pair binding energy defined as

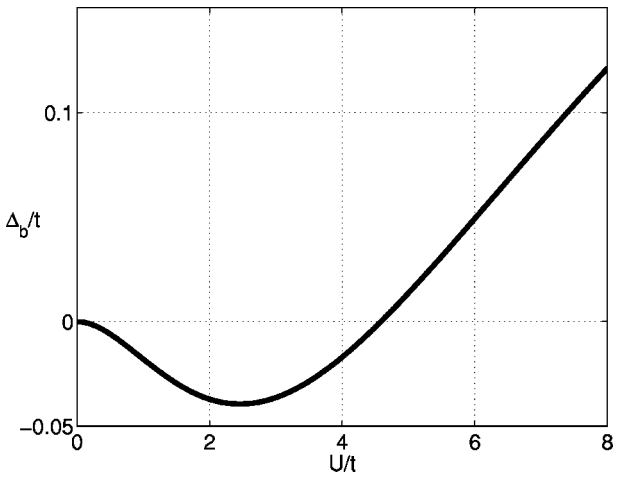

FIG. 4. Pair binding energy on a plaquette. Δ_b of Eq. (15) calculated for the Hubbard model for different interaction strengths. For $\Delta_b<0$ the hole pair is more stable than two single holes on a disconnected plaquette lattice.

$$\Delta_b \equiv E(0) + E(2) - 2E(1), \tag{15}$$

where $E(N_h)$ is the ground state of N_h holes. Δ_b is depicted in Fig. 4. In the range $U/t \in (0,5)$, it is bounded by $-0.04t < \Delta_b < 0$. It has been well appreciated that the Hubbard, t-J and even CuO_2 models have pair binding in finite clusters starting with one plaquette.[18] In larger clusters, such as the 4×4 lattice, pair binding is seen for up to 6 holes[4] (three hole pairs) for $U/t \leqslant 20$. This does not yet explain the integrity of pair correlations on the infinite lattice since the electron hopping energy t is much larger than the pair binding energy. In Sec. IV B and Appendix A, we show numerical evidence that plaquette pairs *survive* disintegration into fermions.

A d-wave superconducting state can be written as the coherent state

$$\Psi^{d\text{-scF}} \equiv \prod_i^{\text{plaq}} (\cos\theta + \sin\theta e^{i\varphi} b^\dagger_i)|\Omega\rangle, \tag{16}$$

with the superconductor order parameter

$$\langle\Psi|d_{ij}c_{i\uparrow}c_{j\downarrow}|\Psi\rangle = \sqrt{Z'_b}e^{i\varphi}\sin\theta\cos\theta. \tag{17}$$

It is worthwhile to reemphasize the following point which has important implications in interpreting both experiments and numerics of Hubbard-like models. The fermions and hole pairs have charges $+e$ and $+2e$ respectively. Their number is counted from the correlated half-filled (RVB) vacuum. The operators f and b should not be confused with the electron and Cooper pair operators $c^\dagger_s$ and $c^\dagger_\uparrow c^\dagger_\downarrow$, respectively, whose numbers are counted up from the electron vacuum. In numerical calculations, it is preferable to use the operator $b^\dagger$, as defined by the Hubbard plaquette eigenstates,

as the superconducting order parameter. It should have larger matrix elements than the customary *d*-wave pairing operator $d_{ij}c_{i\uparrow}c_{j\downarrow}$.

E. Underdoped to overdoped transition

Throughout this paper we restrict ourselves to low doping, i.e., a small number of hole pairs and hole fermions per plaquette. Nevertheless, the plaquette states basis leads us to expect an interesting transition at higher hole doping for the following reason.

When the chemical potential is large enough to bring the hole pair (two electron) state to be lower than the four electron vacuum, a *vacuum crossing* takes place. On a single plaquette, the vacuum crossing is when the levels of zero and one boson intersect. Since hole pairs are somewhat larger in size than a single plaquette, the lattice vacuum crossing should take place at somewhat less than $x=0.25$ holes per square lattice site.

Once the two hole state turns into the new vacuum $|\Omega\rangle'$, all excitations are defined with respect to it using different boson and fermion creation operators. For example, the old RVB vacuum becomes a Cooper pair excitation above the new vacuum:

$$|\Omega\rangle \approx \left(\mathcal{P} \sum_{ij} d_{ij} c_{i\uparrow}^{\dagger} c_{i\downarrow}^{\dagger} + \cdots \right) |\Omega\rangle'. \tag{18}$$

It is plausible that the vacuum crossing is a true quantum phase transition, and not merely a mathematical artifact of using different plaquette bases to construct the same ground state. A candidate for such a phase transition is the restoration of square lattice symmetry, if this symmetry is truly broken by plaquettization in the underdoped regime as mentioned in Sec. III B.

The overdoped side is far from half filling, where effects of the Gutzwiller projection are small. That is to say, the eigenstates can be approximated by applying electron operators to the electron vacuum. With interplaquette hybridization of the two electron plaquette vacua, the ground state can be adiabatically connected to the quarter filled electron Fermi surface. In the absence of superconductivity it will exhibit a *large* (Luttinger-theorem obeying) Fermi surface.

III. CONSTRUCTION OF THE EFFECTIVE HAMILTONIAN

Having described the low lying plaquette states, we are faced with the challenge of constructing an effective Hamiltonian for the full lattice. Motivated by the pair binding on a plaquette, one might initially wish to compute the effective hopping of a hole pair between plaquettes using second order perturbation theory in the interplaquette hopping t'.

This naive approach yields pair hopping of order $J_c \propto t'^2/\Delta_b$. The perturbative expansion is controlled by t'/Δ_b. This suggests failure of perturbation theory for $t'=t \gg \Delta_b$. Indeed, by looking at the exact spectrum of two connected plaquettes, we find that second order perturbation fails in a sizable domain of $t'<t$. Does this imply dissociation of the local bosonic correlations in the translationally invariant lattice? We argue no.

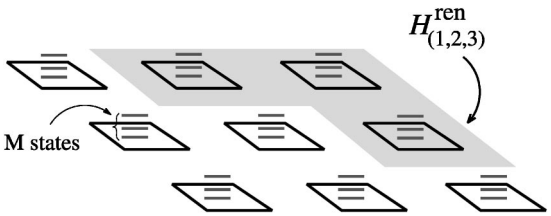

FIG. 5. The reduced Hilbert space of a plaquette cluster used in CORE. The calculation of $H^{\rm ren}_{1,2,3}$ requires diagonalization of the Hubbard model on the cluster highlighted by the shaded region. $H^{\rm ren}$ reproduces the exact spectrum within the reduced Hilbert space.

There is convincing evidence from various numerical approaches, that two holes remain on the same plaquette in $\sqrt{26}\times\sqrt{26}$ lattices[2] and on 8×6 *t-J* ladders.[3] However, in order to understand how many pairs behave on the infinite lattice, we must determine the pair hopping energy, and derive their effective Hamiltonian.

A suitable approach for this task is provided by the contractor renormalization (CORE) method[5] described below. The small parameter of CORE is the ratio of the hole pair separation, i.e., coherence length to the range of the effective interactions.

A. Contractor renormalization algorithm

Given a microscopic Hamiltonian $\mathcal{H}$ on the square lattice we choose a plaquette covering and proceed by the following steps:

Step 1: Defining the reduced Hilbert space. We diagonalize $\mathcal{H}$ on a single plaquette and truncate all states above a chosen cutoff energy. This leaves us with the lowest M states $\{|\alpha\rangle\}_1^M$. The reduced lattice Hilbert space is spanned by tensor products of retained plaquette states $|\alpha_1,\ldots,\alpha_N\rangle$. A case in point is the Hubbard model spectrum, which for the half filled case has 70 states. We truncate 66 states and keep the ground state and lowest triplet, i.e., $M=4$. Thus, the Hilbert space is considerably reduced at the first step.

Step 2: The Renormalized Hamiltonian of a cluster. The reduced Hilbert space on a given connected cluster of N plaquettes is of dimension $\mathcal{M}=M^N$. See Fig. 5 for an illustration. We diagonalize $\mathcal{H}$ on the cluster and obtain the lowest $\mathcal{M}$ eigenstates and energies: $(|n\rangle,\epsilon_n)$, $n=1,\ldots,\mathcal{M}$. The wave functions $|n\rangle$ are projected on the reduced Hilbert space and their components in the plaquette basis $|\alpha_1,\ldots,\alpha_N\rangle$ are obtained. The projected states ψ_n are then Gramm-Schmidt orthonormalized, starting from the ground state upward:

$$|\tilde{\psi}_n\rangle = \frac{1}{Z_n}\left(|\psi_n\rangle - \sum_{m<n} |\tilde{\psi}_m\rangle\langle\tilde{\psi}_m|\psi_n\rangle \right), \tag{19}$$

where Z_n is the normalization. The renormalized Hamiltonian is defined as

$$\mathcal{H}^{\rm ren} \equiv \sum_n^{\mathcal{M}} \epsilon_n |\tilde{\psi}_n\rangle\langle\tilde{\psi}_n|, \tag{20}$$

which ensures that it reproduces the lowest $\mathcal{M}$ eigenenergies exactly.

Representing $\mathcal{H}^{\rm ren}$ in the real space plaquette basis $|\alpha_1,\ldots,\alpha_N\rangle$, defines the (reducible) interplaquette couplings and interactions.

Step 3: Cluster expansion. We define connected N point interactions as

$$h_{i_1,\ldots,i_N}=H^{\rm ren}_{\langle i_1,\ldots,i_N\rangle}-\sum_{\langle i_1,\ldots,i'_N\rangle} h_{i_1,\ldots,i'_N}, \qquad (21)$$

where the sum is over connected subclusters of $\langle i_1,\ldots,i_N\rangle$. The full lattice effective Hamiltonian can be expanded as the sum

$$\mathcal{H}_{\rm eff}=\sum_i h_i+\sum_{\langle ij\rangle} h_{ij}+\sum_{\langle ijk\rangle} h_{ijk}+\cdots \qquad (22)$$

h_i is simply a reduced single plaquette Hamiltonian. h_{ij} contains nearest neighbor couplings and corrections to the on-site terms h_i. h_{ijk} contains three site couplings and so on. $h_{i_1,\ldots,i_N}$ will henceforth be called *range-N interaction*. We expect on physical grounds that for a proper choice of a truncated basis, range-N interactions will decay rapidly with N. This expectation needs to be verified on a case by case basis.

Morningstar and Weinstein, by retaining up to range-3 interactions,[5] demonstrated that the CORE renormalization group flow, obtains an excellent value for the ground state energy of the spin-$\frac{1}{2}$ Heisenberg chain. This is encouraging, since the spin half chain has long range, power-law decaying spin correlations. Pieckarewicz and Shepard[25] tested CORE for the 12 site spin-$\frac{1}{2}$ Heisenberg ladder. They got better than 1% accuracy for all lowest 64 states using a plaquette basis keeping only up to range two interactions.

In general, there is no *a priori* quantitative estimation of the truncation error. Nevertheless, if it decays rapidly with interaction range, we deduce that there is a short *coherence length* related to our local degrees of freedom, e.g., in our case the hole pair bosons and the triplets (bound states of two spinons).

CORE of wave function correlations. The CORE process is designed to reproduce the low lying spectrum, while the wave functions may be significantly distorted during the truncation of the Hilbert space. Does this hinder calculation of correlation functions within this scheme? The answer depends on the operators whose correlations we wish to calculate.

The correlations are calculated by adding external source terms to the original Hamiltonian,

$$\mathcal{H}[\eta]=\mathcal{H}[0]+\sum_i \eta_i\hat{O}_i, \qquad (23)$$

where $\hat{O}_i$ is a microscopic linear perturbation operator whose correlations we wish to determine. We apply the CORE cluster expansion of Eq. (22) to the perturbed Hamiltonian and obtain $\mathcal{H}^{\rm eff}[\eta]$ which is expanded to linear order in η_i,

$$\begin{aligned}\mathcal{H}_{\rm eff}[\eta]&=\sum_j (h_j+\eta_i\hat{O}^{(1)}_{ij})+\sum_{\langle jk\rangle}(h_{jk}+\eta_i\hat{O}^{(2)}_{ijk})\\&\quad+\sum_{\langle jkl\rangle}(h_{jkl}+\eta_i\hat{O}^{(3)}_{ijkl})\cdots+\mathcal{O}(\eta^2)\\&\equiv\mathcal{H}^0_{\rm eff}+\sum_i \eta_i\hat{O}^{\rm eff}_i+\mathcal{O}(\eta^2)\end{aligned}$$

$$\hat{O}^{\rm eff}_i=\hat{O}^{(1)}_i+\sum_j \hat{O}^{(2)}_{ij}+\sum_{jk}\hat{O}^{(3)}_{ijk}+\cdots. \qquad (24)$$

$\hat{O}^{\rm eff}_i$ represents the linear perturbation $\hat{O}_i$ in the truncated Hilbert space

$$\hat{O}^{\rm eff}_i\equiv\sum_{n,m}^{\mathcal{M}}\langle n|\hat{O}_i|m\rangle|\tilde{\psi}_n\rangle\langle\tilde{\psi}_m|. \qquad (25)$$

The two-point dynamical correlation function at low temperature $T\ll\epsilon_{\rm max}$ is given by the Lehmann representation

$$\begin{aligned}S_{ij}(\omega)&\equiv\frac{2\pi}{ZN}\sum_{nm} e^{-\epsilon_n/T}\langle n|\hat{O}_i|m\rangle\langle m|\hat{O}_j|n\rangle\,\delta(\omega+\epsilon_n-\epsilon_m)\\&\simeq\frac{2\pi}{ZN}\sum_{nm}^{\rm trunc} e^{-\epsilon_n/T}\langle\tilde{\psi}_n|\hat{O}^{\rm eff}_i|\tilde{\psi}_m\rangle\langle\tilde{\psi}_m|\hat{O}^{\rm eff}_j|\tilde{\psi}_n\rangle\\&\quad\times\delta(\omega+\epsilon_n-\epsilon_m),\end{aligned} \qquad (26)$$

where Z is the partition function, and the second sum is evaluated in the truncated Hilbert space, using the cluster expansion (24) for the matrix elements.

Thus for the full lattice cluster, $\hat{O}^{\rm eff}_i$ recovers the exact correlations of the *true* low energy eigenstates. By (24) the linearized cluster expansion involves multisite operators

$$\hat{O}^{(n)}_{i,i_1,\ldots,i_n}=\partial h_{i_1,\ldots,i_n}/\partial\eta_i. \qquad (27)$$

A rapid decay of $h_{i_1,\ldots,i_n}$ beyond a short truncation range is essential for the feasibility of the CORE scheme for the spectrum. Similarly, to calculate the correlations of $\hat{O}$, we require a rapid decay of $\hat{O}^{(n)}$ with n, which would allow us to calculate $\hat{O}^{\rm eff}_i$ by small clusters diagonalizations. We have previously argued that a small truncation error results from a short coherence length ξ, for the coarse grained degrees of freedom. For example, the size of the hole pairs in the slightly doped Hubbard model. Thus, the operator $\hat{O}$ should be chosen to have large matrix elements within the reduced Hilbert space, and the multisite operators $\hat{O}^{(n)}_{i_1,\ldots,i_n}$ should decay rapidly beyond the range of ξ.

In other words, if the truncated wave functions retain the relevant local operator content, the cluster expansion for the operators converges rapidly, and the effective Hamiltonian can reproduce the long wavelength correlations correctly. In this paper, the truncated plaquette states, for example, contain d-wave hole pairs on plaquettes. If these hole pairs turn out to be tightly bound in the exact eigenstates of the full lattice, their creation operator has small multisite corrections in the renormalized basis, i.e., it has a rapidly decaying clus-

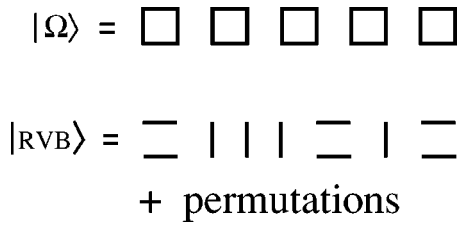

FIG. 6. Restoration of translational symmetry on the ladder. $|\Omega\rangle$ is the plaquette lattice vacuum which breaks twofold lattice translational symmetry. $|\mathrm{RVB}\rangle$ is the dimer resonating valence bonds state which has translational symmetry, and is related to $|\Omega\rangle$ by an exponential of triplet pairs, see Eq. (29).

ter expansion. In this case, long range *d*-wave pair correlations are well represented (up to an onsite renormalization factor), by the boson-boson correlations of the four bosons model.

B. Lattice translational symmetry

The CORE algorithm formally requires explicit breaking of lattice translational symmetry at the first step. The plaquette lattice vacuum breaks lattice translational symmetry as follows: each plaquette vacuum contains a triplet pair contribution, but the product state does not contain interplaquette triplets, and hence differs from the state translated by one square lattice spacing. In order to restore the lattice symmetry, interplaquette triplet pair correlations can be reintroduced by triplet pair creation operators in the effective Hamiltonian.

As an illustration, let us consider the plaquette vacuum of the two leg ladder, in Fig. 6 which can be written in the form

$$|\Omega\rangle = \mathcal{P}\exp\left(\frac{1}{3}\sum_i t^\dagger_{2i\alpha}t^\dagger_{2i+1,\alpha}\right)\prod_i |0\rangle_i, \tag{28}$$

where $|0\rangle_i$ is a singlet on rung *i*, and $t^\dagger_{i\alpha}|0\rangle_i$ is a rung triplet. $\mathcal{P}$ projects out multiple occupation of triplets.

The translational invariant RVB state in Fig. 6, can be constructed from $|\Omega\rangle$ by applying the operator

$$|\mathrm{RVB}\rangle = \mathcal{P}\exp\left(\frac{1}{3}\sum_i t^\dagger_{2i-1\alpha}t^\dagger_{2i,\alpha}\right)|\Omega\rangle. \tag{29}$$

In the triplet bosons representation of the Heisenberg exchange there are anomalous interplaquette terms $t^\dagger_i t^\dagger_i + t_i t_j$. In the mean field theory the Bogoliubov transformation introduces a partial ''symmetry restoring'' exponential operator, which resembles Eq. (29). However symmetry cannot be fully restored to the wave functions in the reduced Hilbert space because of the elimination of higher spin states. Is this a problem? Well, it depends on what one is interested in. CORE is constructed to obtain accurate effective interactions. Unphysical symmetry breaking effects can be introduced by truncating the longer range interactions, as explained by a toy model in Appendix B. Therefore it is hard to *rule out* a physical ''plaquettization'' of the true ground state. Incidentally, such a fourfold discrete symmetry breaking is consistent with Berry phase arguments[26] for the spin liquid phase of spin half Heisenberg models.

The symmetry breaking, appears as minigaps near the edges of the plaquette lattice Brillouin zone (PLBZ) $\kappa_x, \kappa_y \in (-\pi/2, \pi/2)$. In Appendix B, we see how the minigaps of the tight binding model, decrease as longer range interactions are included. For the triplet and hole pair bosons, minigaps do not matter much since their low energy states are around (0,0) and (π,π), respectively; the farthest possible from the PLBZ edges.

On the other hand, low energy fermions happen to be centered around the PLBZ corner $(\pm\pi/2, \pm\pi/2)$, where the effects of plaquette symmetry breaking on the spectrum are large. Although by rotational symmetry, the two bands which contain the $(\pi,0)$ and $(0,\pi)$ states are degenerate at the PBLZ corner, the other two bands have minigaps. These would distort the elliptical shape of the Fermi pockets, an effect which if it exists, could be detected by angular resolved photoemission.

IV. THE PLAQUETTE BOSON-FERMION MODEL

We first start with the bosons, and compute their interplaquette couplings and interactions using CORE. Later we introduce the hole fermions, whose parameters are taken from published numerical data on large clusters, and estimate their coupling to the bosons using symmetry arguments. Finally we discuss the properties of the combined Hamiltonian.

A. Computing boson interactions

For the purpose of this paper, we have limited the CORE calculations to range-2 boson interactions, while projecting out the fermion states. This required a modest numerical diagonalization effort of the Hubbard model on up to eight site clusters. The resulting range-2 four boson model can be separated into bilinear and quartic (interaction) terms

$$\mathcal{H}^{4b} = \mathcal{H}^b[b] + \mathcal{H}^t[t] + \mathcal{H}^{\mathrm{int}}[b,t], \tag{30}$$

where the bosons obey local hard core constraints

$$b^\dagger_i b_i + \sum_\alpha t^\dagger_{\alpha i}t_{\alpha i} \leq 1. \tag{31}$$

The bilinear energy terms are

$$\mathcal{H}^b = (\epsilon_b - 2\mu)\sum_i b^\dagger_i b_i - J_b\sum_{\langle ij\rangle}(b^\dagger_i b_j + \mathrm{H.c.}),$$

$$\mathcal{H}^t = \epsilon_t\sum_{i\alpha} t^\dagger_{\alpha i}t_{\alpha i} - \frac{J_t}{2}\sum_{\alpha\langle ij\rangle}(t^\dagger_{\alpha i}t_{\alpha j} + \mathrm{H.c.})$$

$$-\frac{J_{tt}}{2}\sum_{\alpha\langle ij\rangle}(t^\dagger_{\alpha i}t^\dagger_{\alpha j} + \mathrm{H.c.}). \tag{32}$$

In Fig. 7 we compare the magnitudes of the magnon hoppings J_t, J_{tt} and the hole pair hopping J_b for a range of U/t. First, we observe that $J_t \approx J_{tt} \approx 0.6J$, i.e., the magnon terms have similar form as those previously obtained for the Heisenberg model in the bond operator,[20] and plaquette operator.[27] representations. Second, the region of intersection

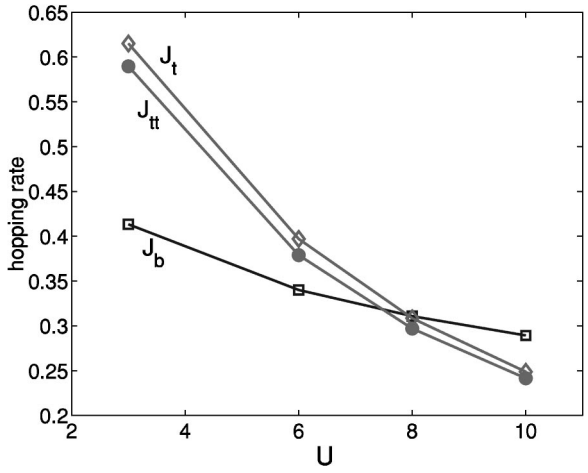

FIG. 7. Boson hopping energies versus Hubbard U. J_t and J_{tt} are the magnon's normal and anomalous hopping energies. J_b is the hole pair hopping energy. The intersection region near $U=8$ is close to the projected SO(5) symmetry point. All energies are in units of t.

near $U/t=8$, is close to the projected SO(5) symmetry point. We emphasize that although there is no quantum SO(5) symmetry in H^{4b}, there is an approximate equality of the bosons hopping energy scales. This equality which was assumed in the pSO(5) theory,[6] previously appealed to phenomenological considerations. Here, the equality emerges in a physically interesting regime of the Hubbard model and has important consequences on the phase diagram as shown below.

$\mathcal{H}^{\text{int}}$ includes nearest neighbor triplet-triplet, pair-pair, and pair-triplet interactions. In Appendix A, $\mathcal{H}^{4b}$ with all its terms is displayed in its full glory, and a table of its computed coupling constants is provided for the values of $U/t=3,6,8,10$. We also compute the truncation error of discarding range-3 terms. This is done by comparing the Hubbard model at $U/t=6$, with 0 and 2 holes on 12 sites, to that of corresponding range-2 $\mathcal{H}^{4b}$. Relative shifts of less than 1% in the ground state and first excitation energies, correspond to a very small truncation error.

B. Mechanism of superconductivity

There are two important effects which together can lead to superconductivity: (i) pairing and (ii) Bose condenstion of the pairs. An important energy scale for both effects is the pair hopping rate J_b.

The small range-3 truncation error was found at a large interaction $U/t=6$, where there is actually no pair binding on a single plaquette (see Fig. 4). The convergence of effective interactions, implies short boson coherence lengths ξ_t, ξ_b. ξ_t is the distance between spinons (localized spin half configurations) which comprise a magnon. ξ_b is the hole pairing distance. Both coherence lengths appear to be of the order of one plaquette size. This conclusion is supported by numerical observation of short distance (lattice constant) correlations between two holes on large lattices.[2,3] It is interesting that the short pair coherence length is dynamically generated in the Hubbard model, even for $U/t>4.5$ where the pair binding energy on an isolated plaquette is positive.

Why is ξ so short? There are two effects which bind pairs: a classical magnetic energy from minimizing the number of broken Heisenberg bonds, and a quantum kinematic pairing for holes moving on two sublattices of a quantum disordered antiferromagnet. The first effect is supported by finding pair binding on a single plaquette. However, this energy also favors clumping many holes together. The quantum pairing effect was proposed by Weigmann, Lee, and Wen, who integrated out spin fluctuations in a quantum disordered phase, to induce a long range electrodynamical attraction between holes on opposite sublattices.[28,29] The kinematic effect produces pairing rather than phase separation, and is robust against additional short range repulsion. It also can explain pair binding on large clusters in a regime of $U/t>4.5$.[18]

Bose condensation. The relative large hopping in the pair kinetic energy $-J_b\Sigma_{\langle i,j\rangle}b_i^\dagger b_j$ is crucial for understanding the cuprate phase diagram.

(i) The pair kinetic energy competes effectively with the antiferromagnetic order. While uncorrelated single fermion kinetic energy is not inhibited by the presence of long range antiferromagnetic order (in fact it strengthens it by a Nagaoka-like mechanism), the pair kinetic energy is substantially lower in a background of short range singlet correlations. This effect was clearly demonstrated in variational Monte Carlo studies of pair kinetic energy in doped RVB wave functions,[30] and is also a property of the variational treatment of the four boson model. The destruction of antiferromagnetic order into a quantum spin liquid with massive triplets, also helps in the kinematical pairing process as discussed above.

(ii) Having destroyed antiferromagnetic order, the pair kinetic energy competes with charge localization due to disorder, or solidification (charge density wave), and with disintegration into unbound hole fermions.

(iii) A large J_b stabilizes a superconducting phase at finite temperatures. It determines the superfluid density $\rho_s=2J_c|\langle b\rangle|^2$, and the phase ordering transition temperature[9] $T_c\approx\rho_s$.

C. Four boson mean field theory

The mean field theory is separated into two parts: (i) Calculation of the order parameters as a function of doping, using variational coherent states. (ii) Determination of magnon resonance energy from a soft interaction version. The results are qualitatively similar to the projected SO(5) phase diagram.[6,31]

Here, we choose $U=8t$, and evaluate the energy of the full boson Hamiltonian (A3), (A4) in the variational coherent states $\psi^{\text{AFM}}(\theta)$ and $\psi^{d\text{-sc}}(\theta)$ of Eqs. (6) and (16), respectively. These states represent the antiferromagnetic and superconducting phase. The critical chemical potential μ_c, where the ground state energies cross, and quantum fluctuation angle $\theta(\mu)$ are determined by minimizing the energy. The spin stiffness and superfluid density are given, respectively, by

$$\rho_{AF}=2J_t\langle t\rangle^2,$$

$$\rho_{SC}=2J_b\langle b\rangle^2, \tag{33}$$

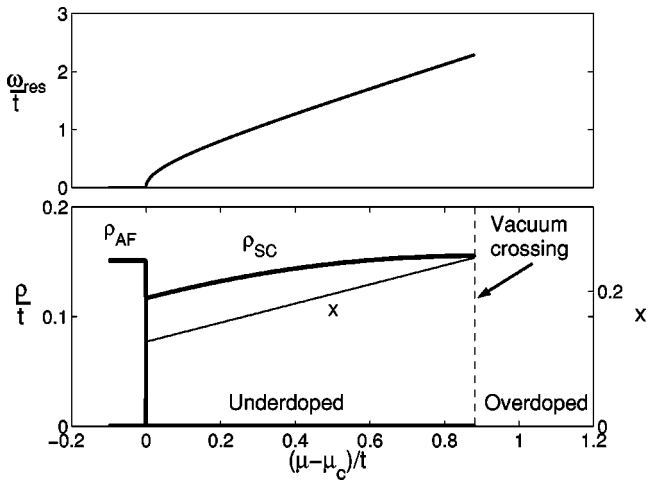

FIG. 8. Variational solution of the four boson model. Results correspond to Hubbard interaction strength $U/t=8$. $\omega_{\rm res}$ is the antiferromagnetic resonance energy, ρ_{AF} is the spin stiffness in the antiferromagnetic phase, and $\rho_{\rm SC}$ is the superfluid density in the superconducting phase. μ-μ_c is the chemical potential difference from the first order transition at μ_c and x is the hole density. The estimated vacuum crossing point is discussed in Sec. II E.

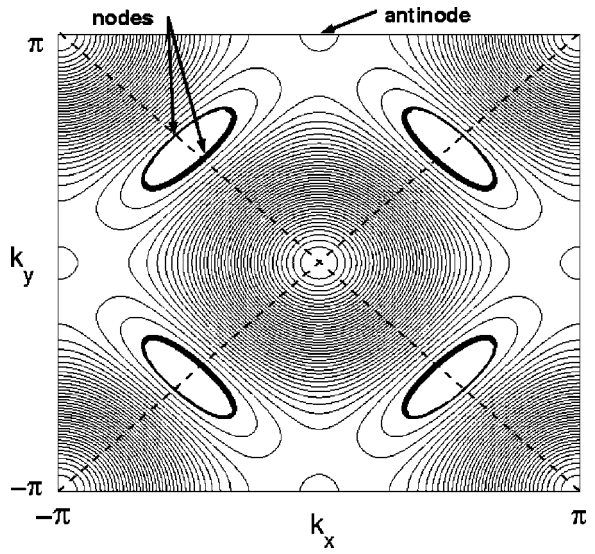

FIG. 9. Hole fermions band structure. Contours of the single hole spectrum Eq. (36) modeled by fitting to published numerical results. For a dilute number of free holes, Fermi pockets will be created around the points $(\pm\pi/2,\pm\pi/2)$. A flat valley near the magnetic zone edge dominates the low energy spectrum.

where we use Eqs. (7), (17) for the magnon and hole pair expectation values. These coefficients, which determine the transition temperatures, as well as the doping concentration x are plotted as a function of chemical potential in Fig. 8. We emphasize that the results should not be quantitatively compared to experiment, since they are variational approximations to a simple model, and neglect effects of low energy hole fermions.

The variational theory yields a first order transition between zero doping and $x_c=x(\mu_c)\approx 0.125$, where the staggered magnetization abruptly vanishes and the superfluid density jumps to a finite value. For charged holes, this first order transition (phase separation), is forbidden by long range Coulomb interactions. Instead one expects high compressibility, incommensurate mixed phases and stripes[32] in the intermediate doping regime $x\in(0,x_c)$.

Even a weak disorder potential is very efficient in breaking the intermediate phase into ''quantum melts,''[33,34] i.e., puddles of superconductor inside antiferromagnetic domains. Above x_c, the superfluid density increases with doping, in agreement with London penetration depth measurements.[8] The overdoped regime is beyond the expected vacuum crossing point (see Sec. II E).

The magnon dispersion in the superconducting phase is obtained by decoupling a soft core interaction[6,31]

$$\mathcal{H}^{\rm int}=W\sum_i :\left(b_i^\dagger b_i+\sum_\alpha t_{\alpha i}^\dagger t_{\alpha i}\right):, \tag{34}$$

where W is fitted to yield the order parameter magnitudes calculated variationally. In the superconductor, the magnons acquire a gap at the antiferromagnetic resonance $\omega_{\rm res}$ which increases with doping as

$$\omega_{\rm res}=2\sqrt{(\mu-\mu_c)(\mu-\mu_c+2J_t)}\propto\sqrt{x-x_c}. \tag{35}$$

This dependence, as plotted in Fig. 8, is qualitatively consistent with inelastic neutron scattering data.[35]

D. Fermion Hamiltonian

In the previous section we have computed the bosonic interactions of Eq. (30) from the Hubbard model using CORE. In that computation, we have eliminated the fermion (single hole) states. We expect, however, that for the two dimensional square lattice, low energy fermion excitations are important. While the fermion holes short range effects on the boson couplings were included in the range-2 CORE calculations, their long wavelength excitations, require diagonalizing larger clusters which are beyond this paper's computational scope. We therefore resort to including the hole fermions dispersion ''by hand,'' i.e., use the single hole band structure computed previously for large clusters. We then estimate their interactions with the bosons.

It is important to emphasize that the definition of the hole pair bosons and the hole fermions is simply a matter of separation: two hole fermions are on *different* plaquettes. When they hop into the same plaquette they turn into one boson via the Andreev coupling defined below.

For the relevant range of U/t the numerically determined band structures for the single hole can be fit by two hopping energies

$$\mathcal{H}^f=\sum_{\mathbf{k}s}(\epsilon_{\mathbf{k}}^f-\mu)f_{\mathbf{k}s}^\dagger f_{\mathbf{k}s},$$

$$\epsilon_{\mathbf{k}}^f=t'[\cos(k_xa)+\cos(k_ya)]^2+t''[\cos(k_xa)-\cos(k_ya)]^2. \tag{36}$$

$\mathbf{k}$ runs over the square lattice Brillouin zone (see Fig. 9). The values $t'\approx J$, and $t''\approx 0.1J$ are taken from the numerical

Quantum Monte Carlo data for the t-J model on a 24×24 lattice,[36] find that for the physically relevant range of $J \in [0.4t, 0.6t]$, the dispersion values are $t' \simeq 0.7J$, $t'' \simeq 0.1t'$.

The magnitude of $t' \approx J$ (rather than the bare value t) and the position of the minima on the magnetic zone edge $(\pi,0)-(0,\pi)$ were explained by theories of holes in the short range antiferromagnetic environment.[37] The semiclassical theory[29] finds that holes are highly dressed local spin polarons, which effectively hop on one sublattice.

From the CORE's perspective, the flat valley between $(\pi,0)$ and $(0,\pi)$ is related to the original degeneracy between the two lowest plaquette fermions. Thus we expect the wave functions of the fermions on the lattice to contain a large component of these two states. Consequences of this on the quasiparticle weight and possible staggered orbital currents were mentioned in Sec. II C.

The holes have hard core interactions among themselves, and with the bosons. At low doping, however, it is still meaningful to describe their states by excitations about small Fermi pockets around $(\pm\pi/2, \pm\pi/2)$.

The fermion density of states of Eq. (36) is plotted in Fig. 11. We see a large peak at low energies (of order $4t'' \ll 4t'$) from the saddle points near the antinodal points. These dominate the hole spectral function, and tunneling density of states at the ''pseudogap'' $\Delta_{\rm pg}$ energy above the chemical potential. Within this framework, $\Delta_{\rm pg}$ does not describe the pairing correlation per se. (It only feels the change in boson density through changes in the common chemical potential). Even in the superconducting phase where hole pairs Bose condense, near antinodal points the Bogoliubov particle-hole admixture is small, and quasiparticles have a character of *holes* in the RVB vaccuum. This has important experimental implications.

(1) Angular resolved photoemission. The large Fermi surface of electrons, given by Hartree-Fock approximations, includes mostly the first magnetic Brillouin zone (the diamond connecting antinodal points). Luttinger's theorem for a Fermi liquid of electrons *excludes* any hole spectral weight outside this area. In contrast, spectral weight of our fermions can be found anywhere outside the small Fermi pockets near $(\pm\pi/2, \pm\pi/2)$. Indeed, broad quasiparticle weight, above T_c has been observed in photoemission data at momenta half way on the line $(\pi,0)\rightarrow(\pi,\pi)$.[12]

A direct evidence of small Fermi pockets would be sharp gapless quasiparticle modes on both sides of $(\pi/2,\pi/2)$. The ''shadow'' quasiparticles closer to (π,π) are harder to observe than the ones closer to (0,0), because of vanishing quasiparticle weight as discussed following Eq. (11).

(2) Tunneling conductance should exhibit an inherent asymmetry between injecting electrons (positive bias) and injecting holes (negative bias). The negative bias peak at the pseudogap voltage is larger than the positive peak, since injecting electrons is suppressed by Hubbard interactions. In other words, electrons can only be injected into existing holes, whose density is of order x, at low doping the ratio of weights should scale with x. A review of (unsymmetrized) tunneling data published by several groups[13,38] reveals such an asymmetry, although we have not seen yet a systematic study of its doping dependence in the literature.

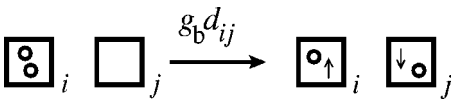

FIG. 10. Andreev coupling between hole pairs and fermions. The microscopic origin of the hole pair-hole fermion coupling is a simple unbinding process. Because of the hole pair d-wave symmetry, the coupling matrix element d_{ij} is odd under $\pi/2$ rotations on the lattice.

E. Boson-fermion couplings

Couplings between bosons and fermions can be derived by microscopic considerations and symmetry. Taking into account the d-wave symmetry of the hole pair state yields an Andreev coupling (see Fig. 10).

$$\mathcal{H}^{bf} = g_b \sum_{\mathbf{k},\mathbf{q}} (d_{\mathbf{k}+\mathbf{q}/2} b_{\mathbf{q}}^\dagger f_{\mathbf{k}\uparrow} f_{-\mathbf{k}+\mathbf{q}\downarrow} + \text{H.c.}), \tag{37}$$

where $d_{\mathbf{k}} = \cos(k_x) - \cos(k_y)$, and $b_{\mathbf{q}}^\dagger = \Sigma_i^{plaq} e^{i\mathbf{q}\cdot\mathbf{x}_i} b_i^\dagger$ is a Fourier component on the plaquette lattice.

In the superconducting phase $\langle b \rangle \neq 0$. This implies a proximity induced pairing of fermions in the small pockets, and an opening of a superconducting gap with the Bogoliubov dispersion

$$E_{\mathbf{k}} = \pm\sqrt{(\epsilon_{\mathbf{k}} - \mu)^2 + \Delta_{\mathbf{k}}^2},$$

$$\Delta_{\mathbf{k}}^{sc} = g_b d_{\mathbf{k}} \langle b \rangle. \tag{38}$$

To be consistent with the range-2 CORE method, we must not include close-by holes on nearest neighbor plaquettes. These excitations were already taken into account in the effective hole pairs hopping energy. The remainder Andreev coupling is therefore between second nearest neighbor hole fermions, with a coupling constant $g_b \leqslant 0.1 J_b$, estimated from the magnitude of the range-3 terms (see Appendix A).

We emphasize that $\Delta_{\rm sc}$ is not the''usual'' BCS gap, since it couples to hole fermions, not electrons. Through its dependence on the Bose condensate order parameter $\langle b \rangle_{Tx}$, we can deduce the transverse quasiparticle velocity at the nodes $v_\perp = \partial\Delta_{\mathbf{k}}/\partial k_\perp$. $v_\perp \rightarrow 0$ at T_c, and it should vary with doping as

$$v_\perp \propto \sqrt{T_c} \propto \sqrt{x}. \tag{39}$$

At higher temperatures than T_c, $\Delta_{\mathbf{k}}$ vanishes and a broadened signature of the small Fermi surface emerges in the spectral function. In contrast, near antinodal points, Bogoliubov particle-hole mixing is negligible and spectral weight is due to hole fermions. This is consistent with photoemission data which finds that above T_c the gap closes only in a small region around the nodal direction.[23]

The Andreev coupling (37) couples the superconducting phase fluctuations to nodal quasiparticles. Similar interactions were used to calculate the temperature dependent London penetration length.[39] That calculation found the fermions

to be more dominant at low temperatures than thermal phase fluctuations in destroying the superfluid density. The effects of this term on the fermions above T_c, were recently argued to give rise to marginal Fermi liquid spectral peaks.[40]

Lastly, the fermion-magnon coupling is given by

$$\mathcal{H}^{tf} = g_t \sum_{ms\mathbf{k}\cdot\mathbf{q}} ((t^{\dagger}_{m\mathbf{q}} + t_{-m-\mathbf{q}}) f^{\dagger}_{\mathbf{ks}} f_{\mathbf{k}+\mathbf{q}+\vec{\pi}s+m} + \text{H.c.}). \tag{40}$$

This singlet interaction term, flips fermion spins and scatters them with momentum (π,π) while emitting or absorbing magnons. It produces signatures of the antiferromagnetic resonance in the fermions self-energy.[41,12] Equation (40) is similar to fermion-magnon terms which were considered for predicting antiferromagnetic resonance signatures in tunneling and photoemission.[42]

F. Boson-fermion thermodynamics

The end result of the previous sections is a system of four bosons and a gas of hole fermions in thermochemical equilibrium, i.e., the charged bosons and fermions share a common chemical potential μ. Combining Eqs. (30), (36), (37), (40) yields the complete plaquette boson-fermion Hamiltonian

$$\mathcal{H}^{\text{PBFM}} = \mathcal{H}^{4b}[2\mu] + \mathcal{H}^{f}[\mu] + \mathcal{H}^{bf} + \mathcal{H}^{tf}. \tag{41}$$

In a uniform phase, the fermions and and hole pair bosons obey a global charge density constraint

$$2n_b(2\mu,T) + n_f(\mu,T) = x. \tag{42}$$

An important missing parameter, in the absence of a consistent calculation of the fermions bands, is the relative position of the lowest fermion and hole pair energies.

Numerical evidence for 4×4 Hubbard clusters[4] show that for up to three hole pairs, there is a negative pair binding energy, i.e., the lowest fermion state at $(\pi/2,\pi/2)$ is still above the boson condensate. However, at finite doping where superconductivity wins over antiferromagnetism, the repulsively interacting bosons may have higher energy than the bottom of the fermion bands. This will produce gapless nodal fermions in the superconductor. Here we shall assume that already at very low doping these energies match, and bosons and fermions coexist.

The boson and fermion compressibilities are

$$\kappa_b = \partial n_b / \partial(2\mu),$$

$$\kappa_f = \partial n_f / \partial\mu, \tag{43}$$

where n_b, n_f are boson and fermion densities per square lattice site. The zero temperature fermion compressibility, up to a Landau parameter correction, is approximately equal to the Fermi pockets density of states, by Eq. (36):

$$\kappa_f \sim \frac{1}{\pi\sqrt{t' t''}}. \tag{44}$$

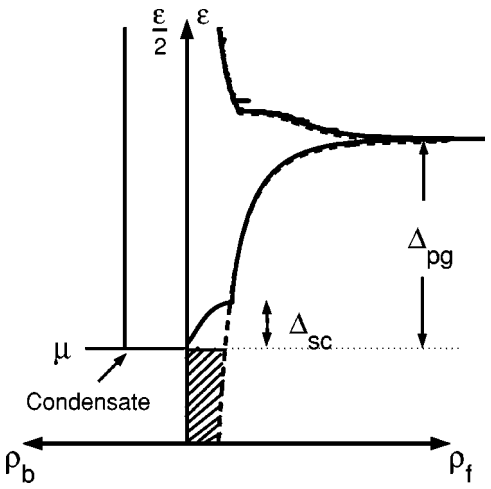

FIG. 11. Hole fermions and hole pair bosons density of states. The fermion density of states is calculated for dispersions Eq. (36) for the normal state (dashed line), and superconducting state Eq. (38) (solid line). The low energy scale t'' creates a large peak in the hole density of states. Hole pair bosons single particle density of states is approximated as a constant corresponding to the noninteracting bilinear terms of H^b in Eq. (32). Δ_{sc} and Δ_{pg} refer to the superconducting gap of Eq. (38) and pseudogap of Eq. (47), respectively.

The boson compressibility (using the xy model representation of hard core bosons) is approximately

$$\kappa_b \sim \frac{1}{32J_b}. \tag{45}$$

At zero temperature, ignoring boson-fermion interactions, we use Eqs. (43) and (42) to obtain the change in chemical potential to linear order in doping x

$$\mu(x) - \mu(0) = \frac{x}{(2\kappa_b + \kappa_f)}. \tag{46}$$

In the underdoped regime, where $x \ll 1$, the energy distance between μ and the fermion saddle points $\mathbf{k}^{\text{SP}} \approx (\pi,0)$ defines the *pseudogap* Δ_{pg} as measured in tunneling and photoemission (see Fig. 11). Its doping dependence is simply connected to the chemical potential shift

$$\Delta_{\text{pg}}(x) = E_{\mathbf{k}^{\text{SP}}} - \mu(x,T), \tag{47}$$

which yields a steady reduction of the pseudogap as a function of doping as plotted in Fig. 12. In the normal state above T_c, we have a theory of two decoupled, noninteracting gases. For the bosons, we use a constant density of states $\rho_b(\omega)$, and for the fermions we choose $\rho_f(\epsilon)$ from the dispersion (36) (see Fig. 11). In this simplified theory, $\mu(T,x)$ can be found using Eq. (42) and solving

$$2\int d\omega \frac{\rho_b(\omega)}{e^{(\omega-2\mu)/T}-1} + \int d\epsilon \frac{\rho_f(\epsilon)}{e^{(\epsilon-\mu)/T}+1} = x. \tag{48}$$

The grand potential and entropy are given by

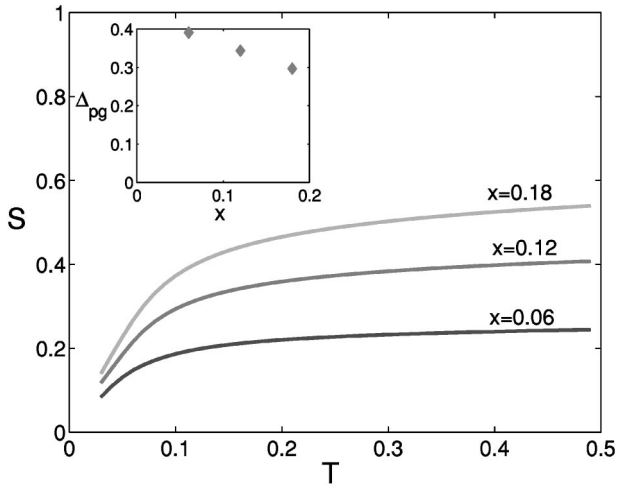

FIG. 12. Thermodynamics of the PBFM. Excess normal state hole entropy as a function of temperature for different doping levels, calculated using Eq. (49). Inset: The pseudogap energy as a function of doping. Energies and temperatures are in units of the holes hopping parameter t' of Eq. (36).

$$\Omega(T) = -T\int d\omega \rho_b(\omega)\ln(1-e^{-[\omega-2\mu(T)]/T}) + T\int d\epsilon \rho_f(\epsilon)\ln(e^{-(\epsilon-\mu)/T}+1),$$

$$S(T) = -\partial\Omega/\partial T. \tag{49}$$

In Fig. 12 the excess hole entropy $S(T,x)$ in the nonsuperconducting state is shown for the density of states given in Fig. 11. The picture which emerges is that above the superconducting transition temperature, bosons *evaporate* into the fermions gas. The evaporation is driven by the larger density of states of hole fermions than the bosons. This evaporation also implies a rapid increase in magnetic susceptibility. Its effects on transport have not yet been calculated.

V. SUMMARY AND DISCUSSION

This paper is primarily aimed at demonstrating the application of CORE to the Hubbard model, which allows us to extract its low energy degrees of freedom and derive the plaquette boson-Fermion model. The CORE calculation could be improved by diagonalizing larger clusters within contemporary computational capabilities. A consistent computation of both the boson and fermion parameters would be useful. It would permit systematic studies of extended Hubbard models and the effects of additional interactions.

The *d*-wave hole pairs are already present in the Hubbard model on a single plaquette. Fortunately, due to the short coherence length and large hopping rate, the pairs maintain their integrity in the square lattice.

The PBFM, at the simplest level of approximation, provides a phase diagram which shares the basic features of underdoped cuprates: the antiferromagnetic Mott insulator and a *d*-wave superconductor with nodal hole fermions. In the superconducting phase, the local spin one magnons are gapped at the antiferromagnetic resonance energy, and the remaining gapless excitations consist of a small density of hole pair bosons and spin half hole fermions. The PBFM brings us closer to understanding low temperature correlations of cuprates. It is amenable to mean field, low density, and variational approximations which do not lend themselves directly to the higher energy Hubbard model and its various extensions.

Here, the PBFM was only preliminarily explored. It would be interesting to study its thermodynamics and transport properties in more detail.

ACKNOWLEDGMENTS

We thank G. Koren, A. Kapitulnik, M. Norman, M. Randeria, S. Sondhi, S. Sachdev, M. Weinstein, and S-C. Zhang for useful discussions. A. A. acknowledges the hospitality of the Institute for Theoretical Physics at Santa Barbara, and Aspen Center for Physics, and support from Israel Science foundation, U.S.-Israel Binational Science Foundation, and the Fund for Promotion of Research at Technion.

APPENDIX A: THE COMPLETE FOUR BOSON MODEL

Here we present the complete four boson model including all interactions generated by CORE up to two plaquette terms. Coupling parameters are listed for square lattice and ladder geometries. We then estimate the magnitude of the truncated three plaquette terms.

The four boson model can be separated into a bilinear part and a quartic part in the bosonic operators

$$\mathcal{H}^{4b} = \mathcal{H}^{b}[b] + \mathcal{H}^{t}[t] + \mathcal{H}^{\rm int}[b,t], \tag{A1}$$

where the bosons obey local hard core constraints

$$b_i^\dagger b_i + \sum_\alpha t_{\alpha i}^\dagger t_{\alpha i} \leqslant 1. \tag{A2}$$

The kinetic (bilinear) terms as written in Sec. IV A are

$$\mathcal{H}^{b} = (\epsilon_b - 2\mu)\sum_i b_i^\dagger b_i - J_b \sum_{\langle ij\rangle} (b_i^\dagger b_j + \text{H.c.}),$$

$$\mathcal{H}^{t} = \epsilon_t \sum_{i\alpha} t_{\alpha i}^\dagger t_{\alpha i} - \frac{J_t}{2}\sum_{\alpha\langle ij\rangle}(t_{\alpha i}^\dagger t_{\alpha j} + \text{H.c.}) - \frac{J_{tt}}{2}\sum_{\alpha\langle ij\rangle}(t_{\alpha i}^\dagger t_{\alpha j}^\dagger + \text{H.c.}). \tag{A3}$$

The higher order interaction terms are

$$\mathcal{H}^{\rm int} = V_b \sum_{\langle ij\rangle} n_{bi} n_{bj} + \sum_{\langle ij\rangle}[V_0 (t_i t_j)_0^\dagger (t_i t_j)_0 + V_1 (t_i t_j)_1^\dagger (t_i t_j)_1 + V_2 (t_i t_j)_2^\dagger (t_i t_j)_2] - J_{bt}\sum_{\langle ij\rangle\alpha}(b_i^\dagger b_j t_{\alpha j}^\dagger t_{\alpha i} + \text{H.c.}) + V_{bt}\sum_{\langle ij\rangle\alpha}(b_i^\dagger b_i t_{\alpha j}^\dagger t_{\alpha j} + b_j^\dagger b_j t_{\alpha i}^\dagger t_{\alpha i}), \tag{A4}$$

TABLE I. Parameters for the four Boson model, in units of t on the square lattice and ladder. The parameters were computed from the Hubbard model using range-2 CORE. Values for the ladder are given in parenthesis where they differ from the square lattice.

	$U=3t$	$U=6t$	$U=8t$	$U=10t$
ϵ_0	-6.613	-8.332	-9.865	-11.549
	(-6.019)	(-7.983)	(-9.593)	(-11.324)
ϵ_t	0.152	0.183	0.174	0.162
	(0.192)	(0.263)	(0.253)	(0.233)
ϵ_b	1.178	2.081	3.557	5.183
	(0.440)	(3.212)	(4.835)	(6.567)
J_t	0.615	0.397	0.309	0.249
J_{tt}	0.590	0.379	0.297	0.242
V_0	-0.361	-0.152	-0.114	-0.099
V_1	-0.203	-0.117	-0.095	-0.082
V_2	0.214	0.099	0.071	0.055
J_b	0.413	0.340	0.311	0.289
J_{bt}	-0.383	-0.233	-0.173	-0.134
V_{bt}	-0.133	-0.286	-0.143	-0.191
V_{bb}	0.884	1.061	1.145	1.213

where $(t_i t_j)^\dagger_S$ creates two triplets on plaquettes i and j, which are coupled into total spin S. When $V_0=2V_1=-2V_2$ the triplet interactions may be written using spin-1 operators as $V_2 \mathbf{S}_i \cdot \mathbf{S}_j$. Similarly, for $J_t=J_{tt}$, which is close to the value given by CORE (see Table I), the bilinear two site triplet terms may be simplified to $J_t \mathbf{n}_i \cdot \mathbf{n}_j$, with $n_\alpha = 1/\sqrt{2}(t^\dagger_\alpha + t_\alpha)$.

The full Hamiltonian (A1) may serve as a starting point for various approximations or numerical studies. Its parameters were computed using CORE from the Hubbard model with $U/t=3,6,8,10$. The parameters are listed in Table I.

Note that the on-site terms for the ladder geometry (given in parentheses in Table I) differ from the square lattice case due to contributions of two plaquette terms h_{ij}. For example let ϵ_t^0 be the bare on site triplet energy from the single plaquette spectrum and $\delta\epsilon_t$ the correction due to the inter-plaquette interaction as described in Sec. III A. The renormalized on-site energy at site i is $\epsilon_t^0 + z_i \delta\epsilon_t$ where z_i is the coordination number of site i. The values of ϵ_t^0 and $\delta\epsilon_t$ may be extracted from the table. For example,

$$\delta\epsilon_t = (\epsilon_t^{\text{square}} - \epsilon_t^{\text{ladder}})/2,$$

$$\epsilon_t^0 = \epsilon_t^{\text{square}} - 4\,\delta\epsilon_t. \tag{A5}$$

TABLE II. Convergence of the cluster expansion. The ratio $\langle h_{ij}\rangle / \langle h_{ijk}\rangle$ given for different sectors in the Hamiltonian with $U=6t$ indicates excellent convergence of CORE on a ladder.

	$S=0$	$S=1$
0 holes	330	7.7
2 holes	27	19.5

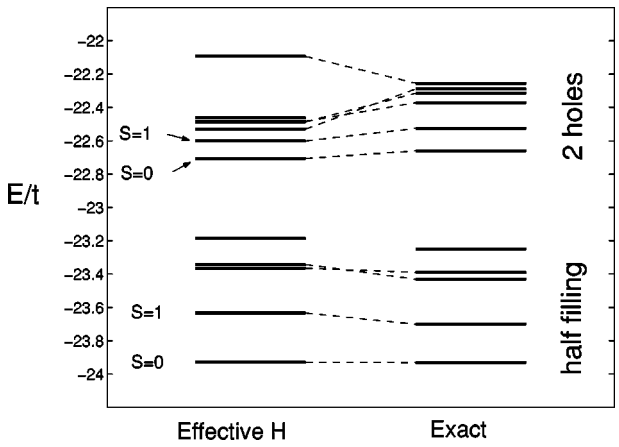

FIG. 13. Low energy spectrum of exact compared to effective Hamiltonian on three plaquettes. The comparison is presented for the Hubbard model with $U=6t$ in the 0-hole and 2-hole sectors. An arbitrary chemical potential was used to set the 2-hole energies slightly above the plotted 0-hole energies.

Estimation of the truncation error. In Fig. 13 we compare between the low energy spectrum of the exact and the truncated effective Hamiltonian for three collinear plaquettes. This comparison may be used to estimate the magnitude of the higher order three plaquette terms h_{ijk} defined by Eq. (21)

$$h_{ijk} \equiv H^{\text{ren}}_{ijk} - (h_{ij} + h_{jk} + h_i + h_j + h_k) = H^{\text{ren}}_{ijk} - H^{\text{eff}}_{ijk}. \tag{A6}$$

Recall that H^{ren}_{ijk} has the exact low lying spectrum of the original Hamiltonian on the three plaquettes. Thus expectation values of h_{ijk} in the ground state and first excited states are calculated by subtracting energies of H^{eff}_{ijk} from corresponding exact energies of the three plaquette problem. We estimate $\langle h_{ij}\rangle$ in a similar way, by comparing energies of two disjoint plaquettes to the exact energies of two coupled

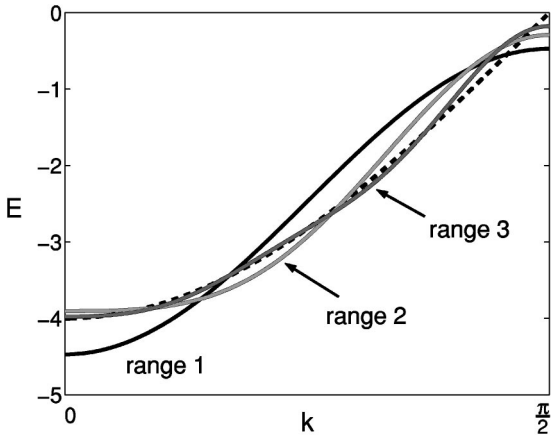

FIG. 14. Tight binding dispersion from a CORE calculation. The model is coarse grained into dimers, and the cluster expansion is truncated at increasing hopping ranges. Away from the dimer Brillouin zone edge, the approximate dispersion (solid lines) converges rapidly to the exact solution (dashed line). Its convergence is much slower at the dimer zone edge.

plaquettes. Small expectation values $\langle h_{ijk}\rangle$ relative to $\langle h_{ij}\rangle$ suggest rapid convergence of the cluster expansion.

Table II gives a summary of the ratios $\langle h_{ij}\rangle/\langle h_{ijk}\rangle$ in the lowest states of the different sectors of the Hamiltonian. The satisfactory convergence of the cluster expansion, implies the integrity of bosonic states on the lattice, at least for ladder geometry. Interestingly, it is still very good for the Hubbard model with $U=6t$ where pair binding energy is positive on a plaquette. This strengthens the argument that binding is generated dynamically on the lattice. The holes remain tightly bound because correlated motion reduces their kinetic energy.

APPENDIX B: CORE CALCULATION FOR THE TIGHT BINDING MODEL

In Sec. III B we discussed the effects of breaking lattice translational symmetry within the reduced Hilbert space. We argued that interactions of increasing range gradually reduce the effects of symmetry breaking on the spectrum. It is instructive to study this process in a simple model where a CORE calculation can be carried easily to long ranges. Such an opportunity is provided by the tight binding model on a chain

$$\mathcal{H}=-\sum_i (c_i^\dagger c_{i+1}+c_{i+1}^\dagger c_i). \tag{B1}$$

We apply CORE to the single electron sector of this model, coarse graining it to blocks of two sites. In each block we retain only the empty state $|0\rangle_i$ and the single electron symmetric state of energy $-t$:

$$f_i^\dagger|0\rangle\equiv\frac{1}{\sqrt{2}}(c_{2i}^\dagger+c_{2i+1}^\dagger). \tag{B2}$$

Hence we can only hope to reconstruct the lowest of the 2 bands in the folded Brillouin zone $k=[-\pi/2,\pi/2]$.

The effective Hamiltonian generated by CORE at any range of the cluster expansion is of the general form

$$\mathcal{H}^{\rm eff}=\sum_{ij} t_{ij}(f_i^\dagger f_j+f_j^\dagger f_i). \tag{B3}$$

Such a Hamiltonian cannot reproduce the sharp band edge at $k=\pm\pi/2$ at any finite range of hopping. However, as demonstrated in Fig. 14, CORE calculations of increasing range introduce higher harmonics that successively approximate the sharp edge. If one is interested in the properties of the model far from the dimerized zone edge then by Fig. 14 the effective Hamiltonian generated by range-3 CORE should suffice.

[1] P.W. Anderson, Science **235**, 1196 (1987).
[2] D. Poilblanc, Phys. Rev. B **49**, 1477 (1994).
[3] S.R. White and D.J. Scalapino, Phys. Rev. B **55**, 6504 (1997).
[4] E. Dagotto, A. Moreo, F. Ortolani, D. Poilblanc, and J. Riera, Phys. Rev. B **45**, 10 741 (1992).
[5] C.J. Morningstar and M. Weinstein, Phys. Rev. D **54**, 4131 (1996).
[6] S-C. Zhang, J-P. Hu, E. Arrigoni, W. Hanke, and A. Auerbach, Phys. Rev. B **60**, 13 070 (1999).
[7] A. Dorneich, W. Hanke, E. Arrigoni, M. Troyer, and S.C. Zhang, cond-mat/0106473 (unpublished).
[8] Y.J. Uemura, G.M. Luke, B.J. Sternlieb, J.H. Brewer, J.F. Carolan, W.N. Hardy, R. Kadono, J.R. Kempton, R.F. Kiefl, S.R. Kreitzman, P. Mulhern, T.M. Riseman, D. Ll. Williams, B.X. Yang, S. Uchida, H. Takagi, J. Gopalakrishnan, A.W. Sleight, M.A. Subramanian, C.L. Chien, M.Z. Cieplak, Gang Xiao, V.Y. Lee, B.W. Statt, C.E. Stronach, W.J. Kossler, and X.H. Yu, Phys. Rev. Lett. **62**, 2317 (1989).
[9] V.J. Emery and S.A. Kivelson, Nature (London) **374**, 434 (1995).
[10] A. Auerbach and E. Altman, Phys. Rev. Lett. **85**, 3480 (2000).
[11] J. Ranninger, J.M. Robin, and M. Eschrig, Phys. Rev. Lett. **74**, 4027 (1995); R. Friedberg and T.D. Lee, Phys. Rev. B **40**, 6745 (1989).
[12] J.C. Campuzano, H. Ding, M.R. Norman, H.M. Fretwell, M. Randeria, A. Kaminski, J. Mesot, T. Takeuchi, T. Sato, T. Yokoya, T. Takahashi, T. Mochiku, K. Kadowaki, P. Guptasarma, D.G. Hinks, Z. Konstantinovic, Z.Z. Li, and H. Raffy, Phys. Rev. Lett. **83**, 3709 (1999).
[13] Ch. Renner, B. Revaz, J.Y. Genoud, K. Kadowaki, and Ø. Fischer, Phys. Rev. Lett. **80**, 149 (1998).
[14] A.G. Loeser, Z.X. Shen, D.S. Dessau, D.S. Marshall, C.H. Park, P. Fournier, and A. Kapitulnik, Science **273**, 325 (1996).
[15] H. Ding, T. Yokoya, J.C. Campuzano, T. Takahashi, M. Randeria, M.R. Norman, T. Mochiku, K. Kadowaki, and J. Giapintzakis, Nature (London) **382**, 51 (1996); H. Ding, J. Phys. Chem. Solids **59**, 1888 (1998).
[16] C. Panagopoulos and T. Xiang, Phys. Rev. Lett. **81**, 2336 (1998).
[17] J.W. Loram, K.A. Mizra, J.R. Cooper, and J.L. Tallon, J. Phys. Chem. Solids **59**, 2091 (1998).
[18] J.E. Hirsch, S. Tang, E. Loh, Jr., and D.J. Scalapino, Phys. Rev. Lett. **60**, 1668 (1988); J.A. Riera and A.P. Young, Phys. Rev. B **39**, 9697 (1989); R.M. Fye, M.J. Martins and R.T. Scalettar, *ibid.* **42**, 6809 (1990).
[19] A. Auerbach, *Interacting Electrons and Quantum Magnetism* (Springer, Berlin, 1994), Chap. 3.
[20] S. Sachdev, R.N. Bhatt, Phys. Rev. B **41**, 9323 (1990); S. Gopalan, T.M. Rice, and M. Sigrist, *ibid.* **49**, 8901 (1994).
[21] I. Bose and S. Gayen, Phys. Rev. B **48**, 10 653 (1993).
[22] K. Park and S. Sachdev, Phys. Rev. B **64**, 184510 (2001).
[23] M.R. Norman, H. Ding, M. Randeria, J.C. Campuzano, T. Yokoya, T. Takeuchi, T. Takahashi, T. Mochiku, K. Kadowaki, P. Guptasarma, and D.G. Hinks, Nature (London) **392**, 157 (1998).
[24] S. Chakravarty, R.B. Laughlin, D.K. Morr, and C. Nayak, Phys. Rev. B **63**, 094503 (2001).
[25] J. Piekarewicz and J.R. Shepard, Phys. Rev. B **56**, 5366 (1997).
[26] F.D.M. Haldane, Phys. Rev. Lett. **61**, 1029 (1988); N. Read and S. Sachdev, *ibid.* **62**, 1694 (1989).

[27] J. Piekarewicz and J.R. Shepard, Phys. Rev. B **60**, 9456 (1999).
[28] P.B. Wiegmann, Phys. Rev. Lett. **60**, 821 (1988); P.A. Lee, *ibid.* **63**, 680 (1989); X-G. Wen, Phys. Rev. B **39**, 7223 (1989).
[29] A. Auerbach and B.E. Larson, Phys. Rev. Lett. **66**, 2262 (1991); See also Ref. 19, Chap. 19.
[30] M. Havilio and A. Auerbach, Phys. Rev. Lett. **83**, 4848 (1999); M. Havilio and A. Auerbach, Phys. Rev. B **62**, 324 (2000).
[31] A. Auerbach and E. Altman, Int. J. Mod. Phys. B **15**, 2509 (2001).
[32] V.J. Emery, S.A. Kivelson, and O. Zachar, Phys. Rev. B **56**, 6120 (1997).
[33] E. Shimshoni, A. Auerbach, and A. Kapitulnik, Phys. Rev. Lett. **80**, 3352 (1998).
[34] C. Howald, P. Fournier, and A. Kapitulnik, Phys. Rev. B **64**, 100504 (2001).
[35] H.F. Fong, P. Bourges, Y. Sidis, L.P. Regnault, J. Bossy, A. Ivanov, D.L. Milius, I.A. Aksay, and B. Keimer, Phys. Rev. B **61**, 14 773 (2000); H.F. Fong, B. Keimer, D.L. Milius, and I.A. Aksay, Phys. Rev. Lett. **78**, 713 (1997).
[36] M. Brunner, F.F. Assaad, and A. Muramatsu, Phys. Rev. B **62**, 15 480 (2000).
[37] C.L. Kane, P.A. Lee, and N. Read. Phys. Rev. B **39**, 6880 (1989); F. Marsiglio, A.E. Ruckenstein, S. Schmitt-Rink, and C.M. Varma, Phys. Rev. B **43**, 10 882 (1991).
[38] Aharon Kapitulnik (private communication).
[39] A. Paramekanti, M. Randeria, T.V. Ramakrishnan, and S.S. Mandal, Phys. Rev. B **62**, 6786 (2000).
[40] M. Franz and Z. Tesanovic, cond-mat/0012445 (unpublished).
[41] M. Eschrig and M.R. Norman, Phys. Rev. Lett. **85**, 3261 (2000).
[42] A. Abanov and A.V. Chubukov, Phys. Rev. Lett. **83**, 1652 (1999).